JOURNAL OF GUIDANCE, CONTROL, AND DYNAMICS
Vol. 24, No. 1, January–February 2001

Synergy Between Global Positioning System Code, Carrier, and Signal-to-Noise Ratio Multipath Errors

Jayanta Kumar Ray and M. Elizabeth Cannon
University of Calgary, Calgary, Alberta T2N 1N4, Canada

Global positioning system code, carrier and signal-to-noise ratio (SNR) measurements are corrupted by multipath signals that can significantly affect the quality of data used for static and kinematic positioning applications. A tool to simulate code, carrier, and SNR multipath errors in a user-defined, multiantenna and multireflector environment for multipath error analysis is developed and described. Various relationships between parameters such as the multipath amplitude, phase, and frequency with the satellite dynamics, antenna–reflector distance, antenna–reflector geometry, and signal frequency are derived. Multipath spatial and temporal correlation are analyzed using simulated and field data. The similarities and differences of code, carrier, and SNR multipath error characteristics are also investigated.

Introduction

MULTIPATH is one of the most significant sources of error in high-accuracy satellite-based applications using differential positioning. Multipath is the phenomenon whereby a signal is reflected or diffracted from various objects in the environment and arrives at the receiver via multiple paths.[1] It can be as large as several meters for the code and several centimeters for the carrier phase with currently available receiver technologies, and it cannot be removed through differential positioning due to its highly localized nature.[2]

Multipath effects on a pseudorandom noise (PRN) ranging receiver were studied by Hagerman.[3] His comprehensive investigation of multipath effects on a delay lock loop (DLL) was further extended, for example, by van Nee,[4] Braasch,[2] and Ray and Cannon.[5] Multipath was experienced by several researchers including Falkenberg et al.[6] and Lachapelle et al.[7] in marine differential global positioning system (GPS) experiments, and Cannon and Lachapelle[8] in static and dynamic land experiments. Tranquilla and Carr[9] observed multipath occurring at various locations, such as rock embankments, high-tension overhead wires, and saltwater/freshwater. Notably, Georgiadou and Kleusberg[10] detected carrier-phase multipath using dual frequency receivers. Similarly, there have been numerous publications[1,11–15] on multipath experiences in various applications.

In this paper code and carrier multipath error characteristics are analyzed by investigating the impact of multipath parameters from a geometrical perspective through simulation models. The effect of multiple reflected signals on a dot-product type of noncoherent DLL discriminator is also analyzed. Furthermore, the code and carrier multipath spatial and temporal correlation and similarities and differences among code, carrier, and signal-to-noise ratio (SNR) multipath errors are investigated using simulation and field data. These analyses will help in assessing multipath errors in a given environment and develop multipath mitigation techniques.

Code Multipath in a Dot-Product Discriminator

Figure 1 shows a block diagram of a typical GPS receiver tracking loop, which consists of a DLL for code tracking and a Costas loop for carrier tracking.[16,17] In practice, the DLL in a GPS receiver generally has a noncoherent type of discriminator.[18,19] An n parallel channel receiver will have n such sets of blocks corresponding to each independent tracking loop.

In a receiver, the digitized intermediate frequency signal is input to each of these parallel channels. The input signal is beat with the locally generated in-phase and quadrature-phase replicas of the carrier. The signal is then correlated with the prompt (P), early (E), and

Dr. Jayanta Kumar Ray joined the Department of Geomatics Engineering as a Ph.D. student in 1997 after leading the global positioning system (GPS) research team at Accord Software and Systems, Bangalore, India. He has been involved in GPS research since 1992 in receiver hardware and software design and development, as well as sensor integration. He holds a B.E. and M.Tech in electronics engineering from the Bangalore University and the Indian Institute of Science, India. He graduated with a Ph.D. in June 2000. He is currently the Manager of Research and Development for Accord Software and Systems, Inc., Virginia.

Dr. M. Elizabeth Cannon is a Professor in the Department of Geomatics Engineering at the University of Calgary where she conducts research and teaching in the area of satellite navigation for land, air, and marine applications. Elizabeth has been involved with global positioning systems since 1984 in both industrial and academic environments and has published over 150 journal and conference papers. Elizabeth holds a B.Sc. in mathematics from Acadia University as well as a B.Sc., M.Sc., and Ph.D. in geomatics engineering from the University of Calgary. Elizabeth is a past president of the U.S. Institute of Navigation.

Received 20 March 2000; revision received 24 July 2000; accepted for publication 31 July 2000. Copyright © 2000 by the American Institute of Aeronautics and Astronautics, Inc. All rights reserved.

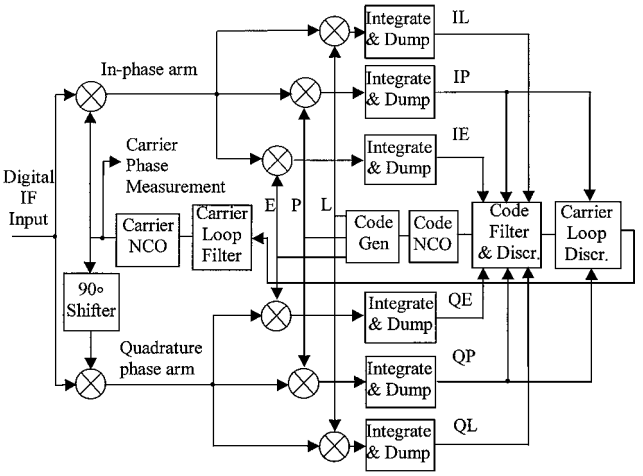

Fig. 1 Typical GPS receiver code and carrier tracking loops.[16,17]

late (L) versions of the locally generated code, and the correlation values are integrated for a predetection integration period. The early and late correlation values in the in-phase (I) and quadrature-phase (Q) arms (IE, IL, QE, and QL) are generally used for code tracking, whereas the P correlation values (IP and QP) are used for carrier tracking. Some code discriminators, such as the dot-product type, use P correlation values as well.

The incoming GPS satellite signal in a receiver consists of a direct signal and, often, more than one reflected signal. Each of these direct and reflected signals consists of a carrier modulated by the code as well as the navigation data bits. Data bits are extracted in the receiver at a later stage and are of no concern as long as the predetection integration periods in the receiver tracking loops are from one data bit boundary to another. The composite input signal, neglecting the navigation data bit and assuming that the multipath signal frequency is the same as the direct signal frequency, can be expressed by the following equation:

$$s_I(t) = A\sum_{i=0}^{n} \alpha_i c(t-\tau_i)\cos(\omega_0 t + \gamma_i) \tag{1}$$

where

A = satellite signal carrier amplitude, V
$c(\,)$ = GPS coarse/acquisition or precise code
n = number of direct and reflected signals
α_i = direct and reflected signal coefficient, where α_0 corresponds to the direct signal and is equal to 1
γ_i = satellite signal carrier phase, where γ_0 corresponds to the direct signal phase, rad
τ_i = satellite signal code delay, where τ_0 corresponds to the direct signal code delay, s
ω_0 = satellite signal carrier frequency, rad/s

The reflected signal carrier phase differs from the direct signal carrier phase by 1) the differential path delay and 2) the change in the phase during reflection. The former of these factors depends on the location of the reflector with respect to the antenna, and the latter is a function of the reflector's physical properties and the angle of incidence as described in the preceding section.

The local replica of the carrier has frequency and phase equal to the receiver's estimate of the incoming satellite signal frequency and phase. Similarly, the locally generated P code has a delay equal to the receiver's estimate of the incoming signal code delay. The locally generated signal, combining code and carrier, in the I arm for the prompt correlator then can be expressed as

$$s_{\mathrm{IP}}(t) = c(t-\hat{\tau}_0)\cos(\hat{\omega}_0 t + \hat{\gamma}_0) \tag{2}$$

where

$\hat{\gamma}_0$ = receiver's estimate of the signal carrier phase, rad
$\hat{\tau}_0$ = receiver's estimate of the direct signal code delay, s
$\hat{\omega}_0$ = receiver's estimate of the signal carrier frequency, rad/s

Then, the IP correlation value, assuming that the incoming and the locally generated carrier frequencies are the same, is given by

$$\mathrm{IP} = \overline{s_i(t)s_{\mathrm{IP}}(t)} = \sum_{0}^{n} \alpha_i \frac{A}{2}(\hat{\tau}_c - \tau_i)\cos(\gamma_i - \hat{\gamma}_c) \tag{3}$$

where $R(\,)$ is the correlation function. For a PRN code without band limitation, it is defined as

$$\begin{aligned} A(\tau) &= 1 - (|\tau|/T), && |\tau| \le T \\ &= 0, && |\tau| > T \end{aligned} \tag{4}$$

where

T = PRN code bit period, s
$\hat{\gamma}_c$ = receiver estimate of the incoming signal carrier phase, rad
$\hat{\tau}_c$ = receiver estimate of the incoming signal code delay, m

Similarly, the IE, IL, QP, QE, and QL correlation values in the presence of multipath are, respectively,

$$\mathrm{IE} = \sum_{0}^{n} \alpha_i \frac{A}{2} R(\hat{\tau}_c - \tau_i + T_d)\cos(\gamma_i - \hat{\gamma}_c) \tag{5}$$

$$\mathrm{IL} = \sum_{0}^{n} \alpha_i \frac{A}{2} R(\hat{\tau}_c - \tau_i - T_d)\cos(\gamma_i - \hat{\gamma}_c) \tag{6}$$

$$\mathrm{QP} = \sum_{0}^{n} \alpha_i \frac{A}{2} R(\hat{\tau}_c - \tau_i)\sin(\gamma_i - \hat{\gamma}_c) \tag{7}$$

$$\mathrm{QE} = \sum_{0}^{n} \alpha_i \frac{A}{2} R(\hat{\tau}_c - \tau_i + T_d)\sin(\gamma_i - \hat{\gamma}_c) \tag{8}$$

$$\mathrm{QL} = \sum_{0}^{n} \alpha_i \frac{A}{2} R(\hat{\tau}_c - \tau_i - T_d)\sin(\gamma_i - \hat{\gamma}_c) \tag{9}$$

For a noncoherent dot-product discriminator, the discriminator function is given by[16]

$$D_n = \mathrm{IP}(\mathrm{IE} - \mathrm{IL}) + \mathrm{QP}(\mathrm{QE} - \mathrm{QL}) \tag{10}$$

In the presence of a single dominant reflector, Eq. (10) can be transformed by using expressions from Eqs. (3–9), to give

$$\begin{aligned} D_{nm} = {} & \sum_{i=0}^{1} \alpha_i R(\hat{\tau}_c - \tau_i)\cos(\gamma_i - \hat{\gamma}_c) \\ & \times \left\{ \sum_{i=0}^{1} \alpha_i R(\hat{\tau}_c - \tau_i + T_d)\cos(\gamma_i - \hat{\gamma}_c) \right. \\ & \left. - \sum_{i=0}^{1} \alpha_i R(\hat{\tau}_c - \tau_i - T_d)\cos(\gamma_i - \hat{\gamma}_c) \right\} \\ & + \sum_{i=0}^{1} \alpha_i R(\hat{\tau}_c - \tau_i)\sin(\gamma_i - \hat{\gamma}_c) \\ & \times \left\{ \sum_{i=0}^{1} \alpha_i R(\hat{\tau}_c - \tau_i + T_d)\sin(\gamma_i - \hat{\gamma}_c) \right. \\ & \left. - \sum_{i=0}^{1} \alpha_i R(\hat{\tau}_c - \tau_i - T_d)\sin(\gamma_i - \hat{\gamma}_c) \right\} \end{aligned} \tag{11}$$

Equation (11) can be expanded and simplified to obtain the following expression:

$$\begin{aligned} D_{nm} = {} & R(\hat{\tau}_c - \tau_0)\{R(\hat{\tau}_c - \tau_0 + T_d) - R(\hat{\tau}_c - \tau_0 - T_d)\} \\ & + \alpha_1^2 R(\hat{\tau}_c - \tau_1)\{R(\hat{\tau}_c - \tau_1 + T_d) - R(\hat{\tau}_c - \tau_1 - T_d)\} \\ & + \{\alpha_1 R(\hat{\tau}_c - \tau_0)[R(\hat{\tau}_c - \tau_1 + T_d) - R(\hat{\tau}_c - \tau_1 - T_d)] \\ & + \alpha_1 R(\hat{\tau}_c - \tau_1)[R(\hat{\tau}_c - \tau_0 + T_d) - R(\hat{\tau}_c - \tau_0 - T_d)]\} \\ & \times \cos(\gamma_0 - \gamma_1) \end{aligned} \tag{12}$$

For continuous tracking, D_{nm} is equated to zero, and the resultant delay error is computed. Equation (12) does not have the term $\hat{\gamma}_c$, which appears in the case of a coherent discriminator function. That means that, in this case (or for that matter, in any noncoherent discriminator), code tracking does not depend on the carrier-phase tracking, as long as the carrier frequency is locked. The multipath error can be computed by assuming that $\tau_0 = 0$; in that case, $\hat{\tau}_c$ is the multipath error.

In the case of multiple reflectors, the upper limit of the summation in Eq. (11) will be equal to the number of reflectors in the environment. When three reflectors are assumed in the environment, Eq. (12) may be expanded and rearranged to give the following expression:

$$
\begin{aligned}
D_{nm} &= R(\hat{\tau}_c - \tau_0)\{R(\hat{\tau}_c - \tau_0 + T_d) - R(\hat{\tau}_c - \tau_0 - T_d)\} + \alpha_1^2 R(\hat{\tau}_c - \tau_1)\{R(\hat{\tau}_c - \tau_1 + T_d) - R(\hat{\tau}_c - \tau_1 - T_d)\} \\
&+ \alpha_2^2 R(\hat{\tau}_c - \tau_2)\{R(\hat{\tau}_c - \tau_2 + T_d) - R(\hat{\tau}_c - \tau_2 - T_d)\} + \alpha_3^2 R(\hat{\tau}_c - \tau_3)\{R(\hat{\tau}_c - \tau_3 + T_d) - R(\hat{\tau}_c - \tau_3 - T_d)\} \\
&+ \alpha_1 R(\hat{\tau}_c - \tau_0)\{R(\hat{\tau}_c - \tau_1 + T_d) - R(\hat{\tau}_c - \tau_1 - T_d)\}\cos(\gamma_0 - \gamma_1) + \alpha_2 R(\hat{\tau}_c - \tau_0)\{R(\hat{\tau}_c - \tau_2 + T_d) - R(\hat{\tau}_c - \tau_2 - T_d)\}\cos(\gamma_0 - \gamma_2) \\
&+ \alpha_3 R(\hat{\tau}_c - \tau_0)\{R(\hat{\tau}_c - \tau_3 + T_d) - R(\hat{\tau}_c - \tau_3 - T_d)\}\cos(\gamma_0 - \gamma_3) + \alpha_1 R(\hat{\tau}_c - \tau_1)\{R(\hat{\tau}_c - \tau_0 + T_d) - R(\hat{\tau}_c - \tau_0 - T_d)\}\cos(\gamma_0 - \gamma_1) \\
&+ \alpha_2 R(\hat{\tau}_c - \tau_2)\{R(\hat{\tau}_c - \tau_0 + T_d) - R(\hat{\tau}_c - \tau_0 - T_d)\}\cos(\gamma_0 - \gamma_2) + \alpha_3 R(\hat{\tau}_c - \tau_3)\{R(\hat{\tau}_c - \tau_0 + T_d) - R(\hat{\tau}_c - \tau_0 - T_d)\}\cos(\gamma_0 - \gamma_3) \\
&+ \alpha_1\alpha_2 R(\hat{\tau}_c - \tau_1)\{R(\hat{\tau}_c - \tau_2 + T_d) - R(\hat{\tau}_c - \tau_2 - T_d)\}\cos(\gamma_1 - \gamma_2) + \alpha_1\alpha_3 R(\hat{\tau}_c - \tau_1)\{R(\hat{\tau}_c - \tau_3 + T_d) - R(\hat{\tau}_c - \tau_3 - T_d)\}\cos(\gamma_1 - \gamma_3) \\
&+ \alpha_1\alpha_2 R(\hat{\tau}_c - \tau_2)\{R(\hat{\tau}_c - \tau_1 + T_d) - R(\hat{\tau}_c - \tau_1 - T_d)\}\cos(\gamma_1 - \gamma_2) + \alpha_1\alpha_3 R(\hat{\tau}_c - \tau_3)\{R(\hat{\tau}_c - \tau_1 + T_d) - R(\hat{\tau}_c - \tau_1 - T_d)\}\cos(\gamma_1 - \gamma_3) \\
&+ \alpha_2\alpha_3 R(\hat{\tau}_c - \tau_2)\{R(\hat{\tau}_c - \tau_3 + T_d) - R(\hat{\tau}_c - \tau_3 - T_d)\}\cos(\gamma_2 - \gamma_3) + \alpha_2\alpha_3 R(\hat{\tau}_c - \tau_3)\{R(\hat{\tau}_c - \tau_2 + T_d) - R(\hat{\tau}_c - \tau_2 - T_d)\}\cos(\gamma_2 - \gamma_3)
\end{aligned}
\tag{13}
$$

Equation (13) is used for simulating the code multipath error due to three reflectors in the environment.

Carrier-Phase Multipath

In a GPS receiver, the carrier phase is measured by accumulating the phase of the locally generated carrier. In the absence of multipath, the local carrier locks onto the direct carrier very accurately, and as a result, the true phase difference between the incoming signal carrier and the locally generated carrier is nearly zero (actually, zero mean) at steady state. In the presence of multipath, however, the composite signal phase shifts from the direct signal phase, and the numerically-controlled-oscillator-generated local carrier locks onto the composite carrier phase, resulting in an error in the phase measurement. This error is equal to the difference between the composite signal carrier phase and the direct signal carrier phase.

When Eqs. (3–9) are used and it is assumed that there is a single dominant reflector and the local carrier frequency is the same as the incoming carrier frequency, the arctan discriminator function can be expressed as[16]

$$
\begin{aligned}
D_r &= \arctan\left(\frac{\mathrm{QP}}{\mathrm{IP}}\right) \\
&= \arctan\left(\frac{R(\hat{\tau}_c - \tau_0)\sin(\gamma_0 - \hat{\gamma}_c) + \alpha_1 R(\hat{\tau}_c - \tau_1)\sin(\gamma_1 - \hat{\gamma}_c)}{R(\hat{\tau}_c - \tau_0)\cos(\gamma_0 - \hat{\gamma}_c) + \alpha_1 R(\hat{\tau}_c - \tau_1)\cos(\gamma_1 - \hat{\gamma}_c)}\right)
\end{aligned}
\tag{14}
$$

The carrier tracking loop tries to minimize D_r during signal tracking, and generally its value will be close to zero (actually, zero mean). When τ_0 and γ_0 are assumed to be zero, $\Delta\Psi = \hat{\gamma}_c - \gamma_0$ is replaced, Eq. (14) is equated to zero, and the proper manipulation is performed, the following expression is obtained:

$$
\Delta\Psi = \arctan\left(\frac{\alpha_1 R(\hat{\tau}_c - \tau_1)\sin\gamma_1}{R(\hat{\tau}_c) + \alpha_1 R(\hat{\tau}_c - \tau_1)\cos\gamma_1}\right) \tag{15}
$$

Here, $\Delta\Psi$ is the difference between the composite signal phase (which is tracked by the receiver) and the direct signal phase; it is, therefore, the carrier-phase multipath error. From Eq. (15), it is clear that the reflection coefficient, multipath delay and the multipath phase are the multipath parameters. These multipath parameters are always defined with respect to the direct signal.

When the same procedure is followed, the carrier-phase multipath due to multiple (in this case three) reflectors is given by

$$
\begin{aligned}
\Delta\Psi = \arctan\{&[\alpha_1 R(\hat{\tau}_c - \tau_1)\sin\gamma_1 + \alpha_2 R(\hat{\tau}_c - \tau_2)\sin\gamma_2 \\
&+ \alpha_3 R(\hat{\tau}_c - \tau_3)\sin\gamma_3]/[R(\hat{\tau}_c) + \alpha_1 R(\hat{\tau}_c - \tau_1)\cos\gamma_1 \\
&+ \alpha_2 R(\hat{\tau}_c - \tau_2)\cos\gamma_2 + \alpha_3 R(\hat{\tau}_c - \tau_3)\cos\gamma_3]\}
\end{aligned}
\tag{16}
$$

This expression is used to simulate carrier-phase multipath errors due to multiple reflectors.

In the case of a single reflector, the multipath error reaches an absolute maximum when the reflected signal phase is perpendicular to the composite signal phase. Then the maximum value is given by

$$
\Delta\Psi = \arcsin\left(\frac{\alpha_1 R(\hat{\tau}_c - \tau_1)}{R(\hat{\tau}_c)}\right) \tag{17}
$$

The reflected signal phases corresponding to the maxima and minima of the error can be computed by differentiating Eq. (15) with respect to γ_1, equating it to zero, and solving for γ_1. When the preceding described steps are performed, it can be determined that the multipath errors reach extreme values (maxima and minima) at

$$
\gamma_1(\max) = \cos^{-1}\left(-\frac{\alpha_1 R(\hat{\tau}_c - \tau_1)}{R(\hat{\tau}_c)}\right) \tag{18}
$$

and

$$
\gamma_1(\min) = 2\pi - \cos^{-1}\left(-\frac{\alpha_1 R(\hat{\tau}_c - \tau_1)}{R(\hat{\tau}_c)}\right) \tag{19}
$$

From Eqs. (18) and (19), it is evident that for weak or long delay reflectors, the maxima and minima take place when the multipath phase is close to 90 and 270 deg. However, for strong and close-by reflectors, the maxima and minima occur at close to 180 deg of the multipath phase.

Unlike code multipath errors, which are largely affected by the predetection bandwidth, carrier multipath errors are not greatly affected by the bandwidth limitation. Lowering the bandwidth has two effects: 1) the code multipath errors depend on the bandwidth and, in turn, affect the carrier multipath errors to a small extent and 2) the change in shape of the prompt correlation triangle affects the carrier multipath errors to a small extent.

SNR Multipath Error

Multipath affects not only the code range and carrier-phase measurements, but also the measured signal power, which is an average of the composite signal power due to the direct and reflected signal

carrier. As the reflected signal relative phase varies with time, the power of the composite signal also varies with time, and so does the measured power.

Note that the code and data bits in the GPS signal do not contribute to the signal power because they merely change the phase of the carrier depending on the modulation technique employed. The signal power with or without the data and code bits remains the same. Therefore, the receiver determines the power of the carrier, not the code and data.

In a receiver, the average signal power is generally measured using the prompt correlators and is given by

$$P = IP^2 + IQ^2 \tag{20}$$

When a uniform antenna gain pattern and a single dominant reflector are assumed, and the values of IP and IQ from Eqs. (3–9) are replaced, the signal power can be found and is given by

$$\begin{aligned} P &= R^2(\hat{\tau}_c) + \alpha_1^2 R^2(\hat{\tau}_c - \tau_1) + 2\alpha_1 R(\hat{\tau}_c)R(\hat{\tau}_c - \tau_1)\cos\gamma_1 \\ &= R^2(\hat{\tau}_c)\left(1 + \alpha_1^2\alpha'^2 + 2\alpha_1\alpha'\cos\gamma_1\right) \end{aligned} \tag{21}$$

where the correlation ratio is

$$\alpha' = \frac{R(\hat{\tau}_c - \tau_1)}{R(\hat{\tau}_c)} \tag{22}$$

From Eq. (21), the average signal power in the receiver is a function of the reflection coefficient, multipath delay, and multipath phase. This equation is used for SNR multipath simulation.

Multipath from a Geometrical Perspective

In Fig. 2, a typical multipath scenario is shown, whereby A0 to A4 are several antennas placed close together in a multiantenna system, and the reflections from two sources to A0 are shown. The other four antennas will also be affected by the reflected signals in a similar way.

In Fig. 2, θ and φ are the elevation and azimuth of the direct signal to the antenna, whereas θ_k and φ_k are the elevation and azimuth of the kth reflected signal to the antenna. The distance between the antenna and the reflector in the horizontal plane is d_k, where k is a particular reflector.

Two distinct scenarios are shown in Fig. 2. In the first case (reflector 1), the antenna (A0) is closer to the satellite compared to the reflector, whereas in the second case (reflector 2), the reflector is closer to the satellite compared to the antenna (A0). These two cases are generalized situations and representative of all of the possible scenarios of the antenna–reflector geometry.

Because the satellite is approximately 20,000 km above the Earth, the GPS signal can be assumed to travel as parallel rays to the Earth's surface. A plane wave front perpendicular to the line of sight can be assumed to have the same carrier phase. When this plane intersects

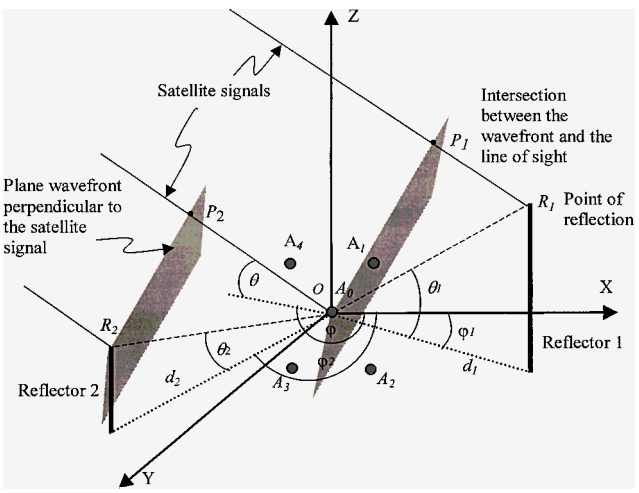

Fig. 2 Direct and reflected signals to an antenna in a multiantenna system.

the phase center of antenna 0, it has the same carrier phase at all points on it, including point P_1 (which is the intersection of the plane and the line of sight from reflector 1 to the satellite). Therefore, the differential path delay of this reflected signal with respect to the direct signal is $\overline{P_1R_1} + \overline{R_1O}$. The corresponding differential phase delay is computed by dividing the differential path delay by the signal wavelength. This assumes no phase change due to reflection of the signal. This assumption is acceptable to characterize multipath errors and their dependency on geometry in a relative sense. To determine the absolute multipath errors, however, the phase change due to reflection of the signal should be accounted for.

Similarly, for case 2, a plane perpendicular to the line of sight from reflector 2 to the satellite intersects the line of sight from the antenna under consideration at point P_2. In this case, the differential path delay is given by $\overline{R_2O} - \overline{P_2O}$.

Therefore, if the direct signal phase at the antenna is available, the reflected signal phase can be computed by adding the differential phase delay due to the differential path delay (under the mentioned assumption) to the direct signal phase.

To compute the effects of multipath, the mentioned differential path delays need to be formulated by a mathematical expression. Using solid geometry, it can be shown that the differential path delay in either situation is given by (see the Appendix)

$$a_k = d_k[(1/\cos\theta_k) - \tan\theta_k \sin\theta - \cos\theta\cos(\varphi - \varphi_k)] \tag{23}$$

where

a_k = differential path delay of the kth reflected signal, m
d_k = horizontal distance between the antenna and the kth reflector, m
θ = elevation of the direct satellite signal, rad
θ_k = elevation of the kth reflected signal, rad
φ = azimuth of the direct satellite signal, rad
φ_k = azimuth of the kth reflected signal, rad

The differential path delay expression is a function of the satellite elevation and azimuth, the reflected signal elevation and azimuth, and the antenna–reflector distance in the local level horizontal plane. This expression is further exploited to analyze the behavior of the carrier-phase multipath error.

With the assumption that the multipath phase is only due to the differential path delay, it can be expressed as

$$\gamma_{0k} = \gamma_k - \gamma_0 = 2\pi a_k/\lambda_L \tag{24}$$

where

γ_k = kth reflected signal phase at the antenna phase center, rad
γ_0 = direct signal phase at the antenna phase center, rad
λ_L = wavelength of the carrier, m

The multipath error is directly related to the multipath phase. The multipath error variation is due to the variation in the multipath phase or the differential path delay. The multipath frequency depends on the rate of change of the multipath phase, or the differential phase delay. The multipath frequency due to a single dominant reflector may be computed by taking the time derivative of the multipath phase expression from Eqs. (23) and (24) and is given by

$$\begin{aligned} \frac{\delta\gamma_{01}}{\delta t} = \frac{2\pi d_1}{\lambda_L}\Bigg(&\{\sin\theta\cos(\varphi - \varphi_1) - \cos\theta\tan\theta_1\}\frac{\delta\theta}{\delta t} \\ &+ \{\cos\theta\sin(\varphi - \varphi_1)\}\frac{\delta\varphi}{\delta t}\Bigg) \end{aligned} \tag{25}$$

Equation (25) relates the multipath error frequency with satellite dynamics. The expression is obtained under the assumption that the antenna–reflector geometry (defined by d_1, θ_1, and φ_1) does not change significantly over the period under consideration. This assumption does not generally hold for kinematic receivers, where the antenna–reflector geometry may change rapidly. Furthermore, in stationary situations, the antenna–reflector geometry changes can

be taken care of by taking the partial derivatives with respect to the reflected signal elevation and azimuth in Eq. (23).

It is evident from Eq. (25) that the multipath error frequency is 1) directly proportional to the distance between the antenna and the reflector, 2) inversely proportional to the wavelength of the carrier signal, 3) directly proportional to the rate of change of elevation of the satellite, 4) directly proportional to the rate of change of azimuth of the satellite, and 5) dependent on the antenna–reflector and the line-of-sight vectors.

Simulation Description

A multipath simulation and mitigation software (MultiSiM) for the GPS was developed using the C programming language on a personal computer platform. The software consists of two main parts, namely, simulation and mitigation. The first part allows the user to define the multipath environment and the antenna setup through the input parameters. The second part, on the other hand, uses various multipath mitigation schemes to reduce the simulated multipath errors.

The major inputs to the simulator are reflector parameters and antenna parameters. The major outputs from the simulator are true range and phase, measured range and phase contaminated with multipath and receiver noise, and estimated range and phase.

The user can input the number of reflectors per satellite and their locations with respect to the antenna position to simulate a controlled multipath environment. The user can also configure the antenna setup, that is, the number of antennas in the antenna array, absolute position of one of the antennas (the reference antenna), and relative positions of all other antennas (secondary antennas) with respect to the reference antenna.

The range and phase of the direct and reflected signals at each antenna may be determined by computing the distance traveled by the signal up to the antenna. For the direct signal, it is the distance between the satellite and the antenna, whereas for the reflected signals, it is the total distance from the satellite to the reflector, plus the reflector to the antenna. The phases of the direct and reflected signals are assumed to be only a function of the ranges and are computed directly from the ranges. The possible change in phase due to reflection of the signal is not considered in this simulation. The satellite position is determined from stored ephemeris data.

The noiseless measured code range is the sum of the direct range between the antenna and the satellite and the code multipath error. The code multipath error is computed by using Eq. (13) and finding the difference between the zero crossings of the multipath-corrupted discriminator function and the multipath-free discriminator function. A single observation from the direct and the numerous reflected signals is generated per satellite–antenna combination.

The measured carrier phase without noise contains two parts: the integer and fractional cycle components. When the direct signal is assumed to be stronger than the indirect signal, the integer cycles in the measured carrier phase are the same as the direct signal's integer cycles. The phase of the fractional cycle of the reflected signal is what actually corrupts the phase of the fractional cycle of the direct signal, depending on its relative strength and phase. Equation (16) is used to compute the multipath error on the fractional part of the carrier phase.

Simulation and Field Results

Multipath Error Versus Reflector Location

Figures 3a–3c show code multipath errors due to one, two, and three reflectors, respectively. For the case of a single reflector at a distance of 15 m (multipath delay 3.6 m) from the antenna, and a reflection coefficient of 0.5, the multipath error is uniform and has slow variations in periodicity due to satellite dynamics (Fig. 3a). The reflector and the antenna positions were assumed to be stationary during the simulation. In the presence of a second reflector at a distance of 50 m (multipath delay 55.2 m) from the antenna, and reflection coefficient of 0.2, the multipath error becomes quite irregular (Fig. 3b). The effect of the second reflector is quite significant in spite of a lower reflection coefficient. This is because, from the code multipath error envelope, reflection from a close-by object produces small multipath errors and, therefore, is less dominant compared to multipath due to a farther object.[2] The addition of a third reflector at a distance of 20 m (multipath delay 30.1 m) from the antenna, and a reflection coefficient of 0.2, have made the multipath error more irregular (Fig. 3c).

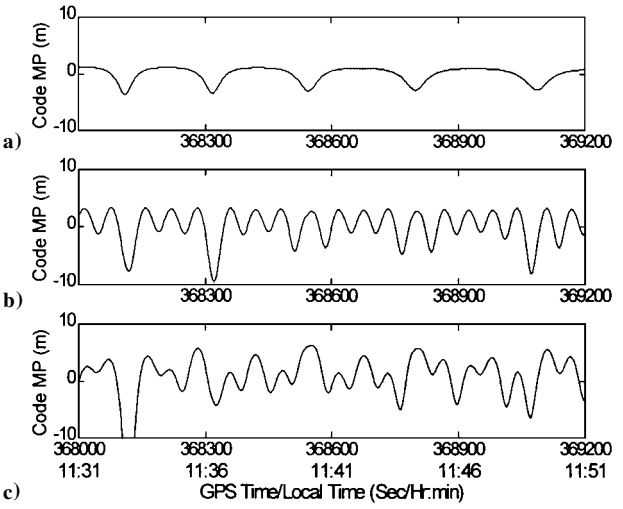

Fig. 3 Code multipath error, where $\alpha_1 = 0.5$, $\alpha_2 = 0.2$, $\alpha_3 = 0.2$, $d_1 = 15$ m, $d_2 = 50$ m, $d_3 = 20$ m, $a_1 = 3.6$ m, $a_2 = 55.2$ m, and $a_3 = 30.1$ m, due to a) one reflector, b) two reflectors, and c) three reflectors.

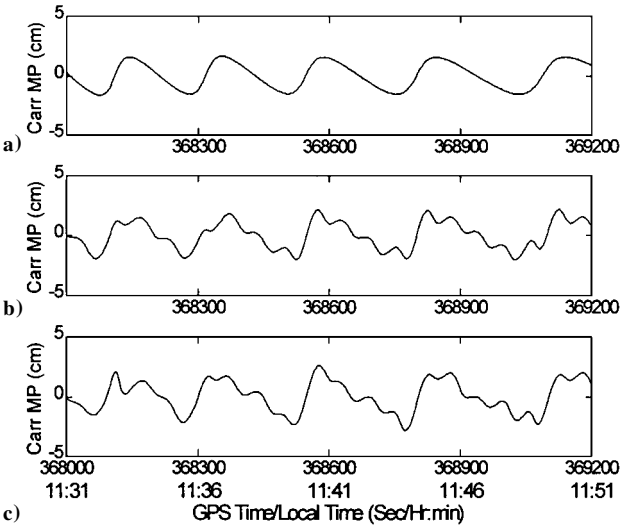

Fig. 4 Carrier phase multipath error, where $\alpha_1 = 0.5$, $\alpha_2 = 0.2$, $\alpha_3 = 0.2$, $d_1 = 15$ m, $d_2 = 50$ m, $d_3 = 20$ m, $a_1 = 3.6$ m, $a_2 = 55.2$ m, and $a_3 = 30.1$ m, due to a) one reflector, b) two reflectors, and c) three reflectors.

Figures 4a–4c show carrier phase multipath errors due to one, two, and three reflectors, respectively, as described in the preceding paragraph (corresponding to Figs. 3a–3c). For the case of a single reflector, the multipath error is regular and has a slow variation in periodicity (Fig. 4a). In the presence of a second reflector, the multipath error pattern does not change significantly compared to the code multipath case (Fig. 4b). This is also evident in the presence of a third reflector (Fig. 4c). The reason for the second and third reflectors having a less significant contribution in the carrier phase case can be explained from the carrier-phase multipath error envelope.[2,4] Unlike the code, the carrier-phase multipath error amplitude proportionately decreases as the multipath delay increases. Multipath delays in the cases of second and third reflectors are longer than the case of the first reflector. Furthermore, the reflection coefficient of the first reflector is higher than the other two, which makes the first reflector the dominant reflector in this case.

Multipath Spatial Correlation

Figures 5a–5e show simulated code multipath errors due to three reflectors at five closely spaced antennas, which are placed 5–10 cm

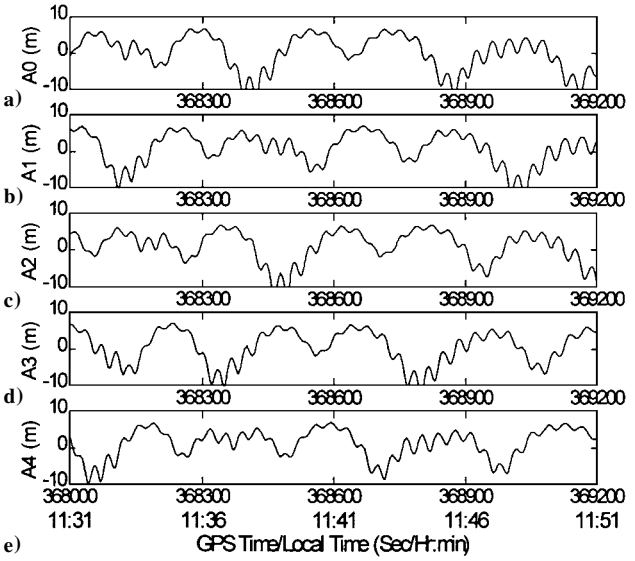

Fig. 5 Code multipath error in five closely spaced antennas due to three reflectors: $\alpha_1 = 0.4$, $\alpha_2 = 0.3$, $\alpha_3 = 0.2$, $d_1 = 10$ m, $d_2 = 30$ m, $d_3 = 56$ m, $a_1 = 8.8$ m, $a_2 = 26.2$ m, and $a_3 = 54.4$ m.

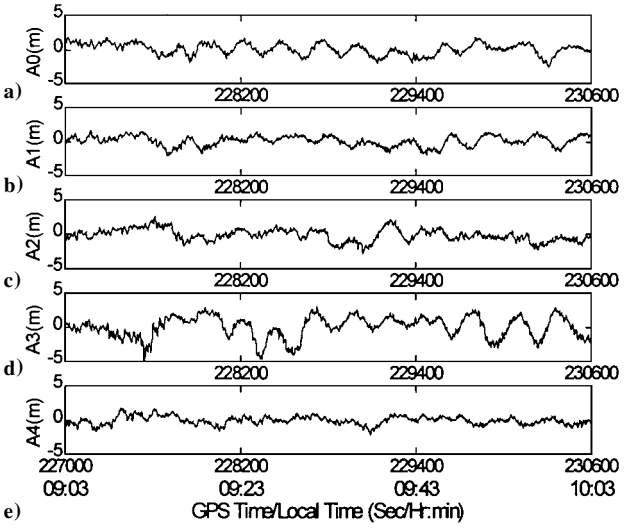

Fig. 6 Code multipath errors in five closely spaced antennas for satellite 31 on 20 Oct. 1998.

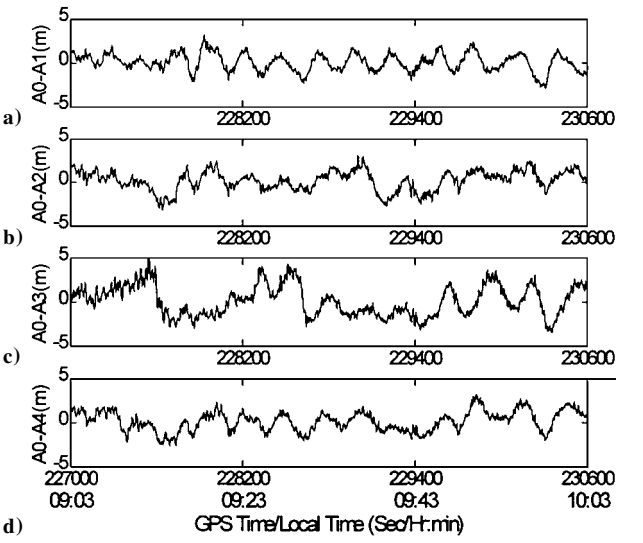

Fig. 7 Single differenced code multipath errors in five closely spaced antennas for satellite 31 on 20 Oct. 1998; A0− A*n* denotes single difference between antennas 0 and *n*.

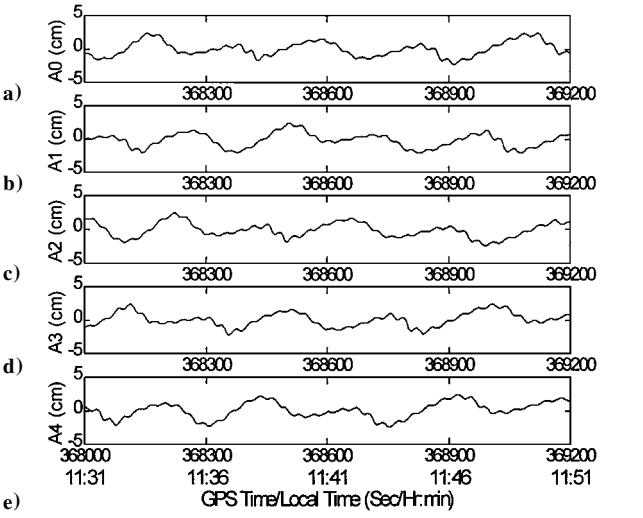

Fig. 8 Carrier phase multipath error in five closely spaced antennas due to three reflectors: $\alpha_1 = 0.4$, $\alpha_2 = 0.3$, $\alpha_3 = 0.2$, $d_1 = 10$ m, $d_2 = 30$ m, $d_3 = 56$ m, $a_1 = 8.8$ m, $a_2 = 26.2$ m, and $a_3 = 54.4$ m.

from each other. It is assumed that the size of the reflector is much higher compared to the largest distance among the antennas, such that all of the antennas in the multiantenna assembly are affected by the same reflector. It is clear from Fig. 5 that the multipath errors are highly correlated between antennas and have very similar patterns. However, they have different phases due to different differential path delays (hence, different multipath phases) of the reflected signal. Because of these phase differences, multipath errors do not get cancelled by taking a single difference of the errors in two closely spaced antennas.

This is further confirmed using field data. The data were collected on the roof of the Engineering Building of the University of Calgary using NovAtel BeeLine™ receivers.[20] It is a moderate multipath environment with reflections coming from the concrete roof and four surrounding walls. Figures 6a–6e show code multipath errors for satellite 31 from data collected on 20 October 1998 on five closely spaced antennas separated by 5–10 cm. Multipath errors for the antennas are generally consistent; however, unlike simulated multipath errors, the errors in each antenna are not due to the same set of reflectors. Furthermore, the multipath phase changes are not smooth due to the irregular and complex environment compared to the simulated environment. These are the primary reasons for the dissimilarities in the multipath patterns in the closely spaced antennas. The multipath errors in the antennas do not cancel out through single differencing between the errors in two antennas, which is demonstrated in Figs. 7a–7d. However, their relationships can be exploited to estimate the multipath error at individual antennas, as described by Ray et al.[21]

Similar to the code multipath error case, Figs. 8a–8e show simulated carrier multipath errors at the same closely spaced antennas. It is clear from Figs. 8 that the multipath errors are highly correlated. However, they do not cancel out by single differencing across two antennas. This is reconfirmed using field data. Figures 9a–9e show carrier multipath errors for satellite 31 from the same field data described earlier. Figures 10a–10d show the single differences of the carrier-phase multipath errors between the antennas. It is evident from Figs. 10 that multipath errors are not the same even for two antennas separated by a small distance. The relationship between multipath errors in closely spaced antennas can be used to estimate the carrier-phase multipath errors in each antenna as described in Refs. 22 and 23.

Multipath Repeatability and Temporal Correlation

Multipath repeatability and temporal correlation was examined for the code and carrier cases. The data collected on the roof of the Engineering Building as described earlier was used for the investigation. The code multipath error was extracted for satellite 31

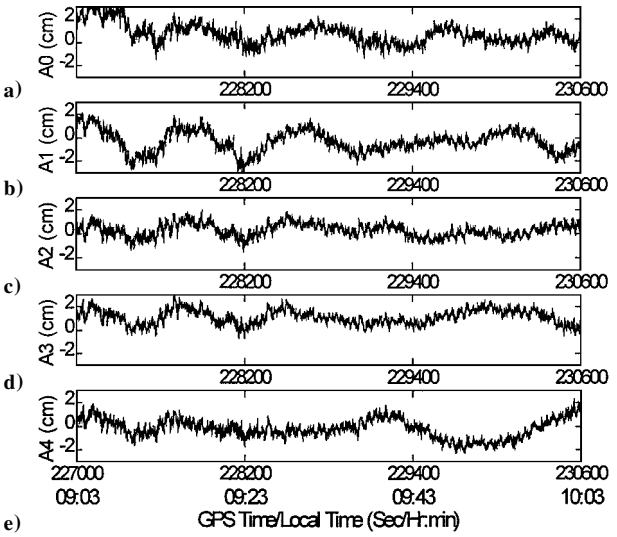

Fig. 9 Carrier phase multipath errors in five closely spaced antennas for satellite 31 on 20 Oct. 1998.

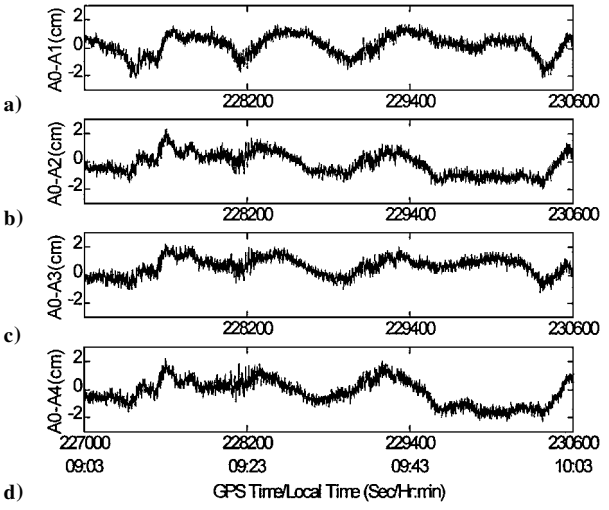

Fig. 10 Single differenced carrier phase multipath errors in five closely spaced antennas for satellite 31 on 20 Oct. 1998; A0– A*n* denotes single difference between antennas 0 and *n*.

(elevation angle 21–34 deg) from data collected on 7 and 8 October 1998 and is shown in Fig. 11 using a shaded dark line and shaded light line for the two days. Multipath errors extracted from the data on 8 October are plotted and are offset by approximately 4 min with respect to the errors extracted from the data collected on 7 October. As the sidereal day is approximately four less than 24 h and the antenna–satellite and antenna–reflector geometry repeat exactly after a sidereal day, the multipath errors should repeat after a sidereal day. From Fig. 11, it is clear that multipath errors repeat to a great extent after a sidereal day.

Figure 12 shows the cross-correlation function of the code multipath errors on 7 October and 8 October for satellite 31. From Fig. 12 it can be seen that the multipath errors have maximum correlation after a sidereal day. The extent of the repeatability is approximately 90% for satellite 31. A correlation time of approximately 2–3 min was found in this case.

The carrier-phase multipath errors for satellite 31 were computed using data collected on 7 October 1998 and are shown in Fig. 13 using a shaded dark line. Similarly, the multipath errors for the same satellite was computed using 8 October data and is superimposed on Fig. 13 but shifted by approximately 4 min in the time (shown using a shaded light line). From Fig. 13, it is clear that the carrier-phase multipath errors repeat after a sidereal day.

Figure 14 shows the cross-correlation function of the carrier-phase multipath errors on 7 October and 8 October for satellite 31.

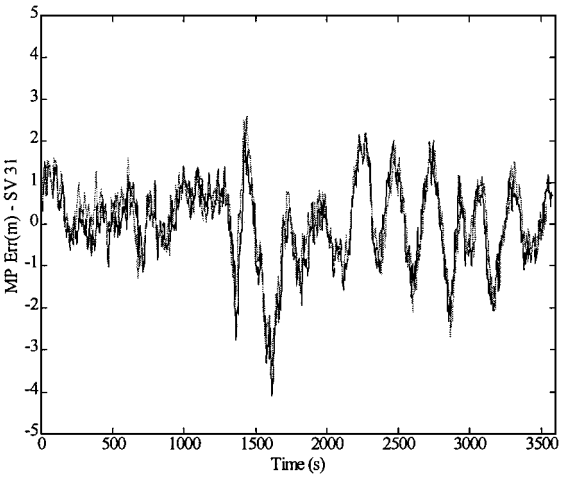

Fig. 11 Code multipath errors for satellite 31 on 7 Oct. 1998 shown in shaded dark line and on 8 Oct. 1998 shown in a shaded light line.

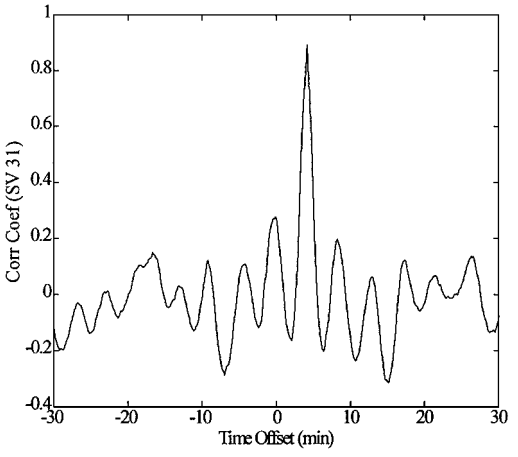

Fig. 12 Correlation coefficients of code multipath errors for satellite 31 using the data collected on 7 and 8 Oct. 1998.

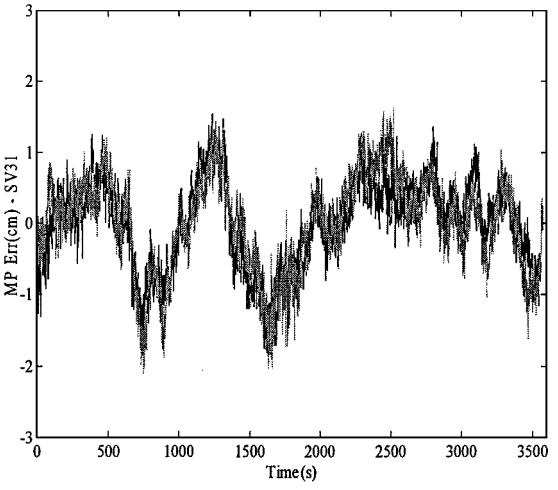

Fig. 13 Carrier phase multipath errors for satellite 31 on 7 Oct. 1998 shown in shaded dark line and on 8 Oct. 1998 shown in a shaded light line.

From Fig. 14, it can be seen that the multipath errors have a maximum similarity after a sidereal day. The extent of the repeatability is approximately 70% in this case. A correlation time of approximately 5–6 min was found in this case.

Comparing the code and carrier multipath errors in Figs. 12 and 14 and Figs. 3c and 4c several comments can be made.

First, code multipath errors have higher frequency components compared to the carrier phase. This is because the code and carrier discriminator functions in the receiver tracking loops respond

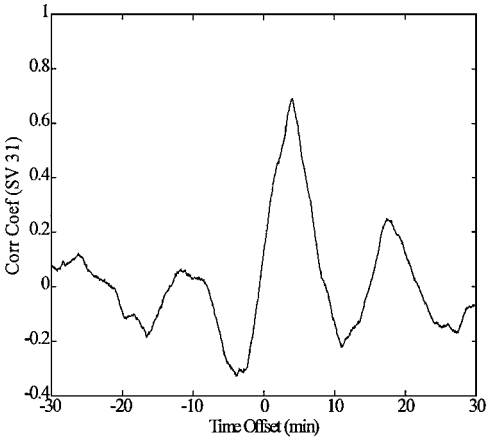

Fig. 14 Correlation coefficients of carrier phase multipath errors for satellite 31 using the data collected on 7 and 8 Oct. 1998.

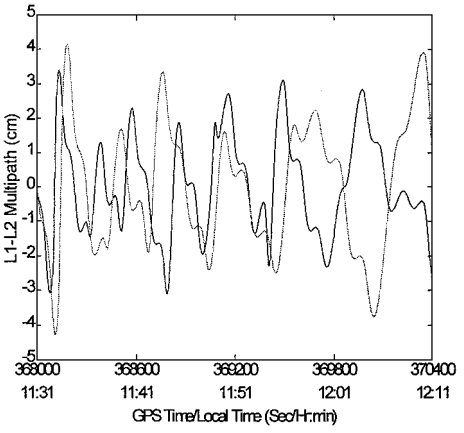

Fig. 15 L1 and L2 carrier phase multipath errors due to three reflectors in a dark and light shaded line, respectively: $\alpha_1 = 0.5$, $\alpha_2 = 0.3$, $\alpha_3 = 0.2$, $d_1 = 15$ m, $d_2 = 30$ m, $d_3 = 20$ m, $a_1 = 3.6$ m, $a_2 = 14.6$ m, and $a_3 = 32.0$ m.

differently in the presence of multipath signals. The code discriminator produces multipath errors of high magnitude due to distant reflectors, which causes high-frequency multipath. Therefore, the code multipath error is dominated by high-frequency components. On the other hand, the carrier discriminator produces multipath errors of high magnitude due to close-by reflectors, which cause low-frequency multipath errors. From Figs. 11 (or 3c) and 13 (or 4c), it can be seen that the dominant reflectors in the code and carrier multipath errors are not the same. For code multipath errors, it is the far away reflectors, whereas for carrier multipath errors, it is the close-by reflectors that dominate the composite multipath errors.

Second, the correlation coefficients (a measure of the day-to-day repeatability) for code multipath errors are higher than those of the carrier phase. This is because the carrier-phase residuals have high phase noise because they are double-differenced residuals. Therefore, the effects of the carrier noise are higher compared to that of the code noise on the correlation coefficient. Because the receiver noise on day one is uncorrelated with the noise on day two, code residuals, which are comparatively less affected by the code noise, have higher correlation coefficients compared to their carrier-phase counterparts.

Multipath Error Versus Carrier Frequency

Figure 15 shows simulated multipath errors in L1 and L2 carriers due to three reflectors. In Figs. 15, the dark shaded errors correspond to the L1 carrier and the light shaded errors to the L2 carrier. Several important observations can be made from Figs. 15. 1) The multipath error has the same amplitude (in radians) for the L1 and L2 carrier (although when multiplied by the wavelength to convert the error into units of distance, the L2 multipath error has a larger amplitude than that of L1). 2) The multipath error has a different phase for the L1 and L2 carrier. At a particular instant, the multipath error for the L1 and L2 carriers look arbitrary, but over a time span, it becomes evident that the error signals have similar patterns. The multipath error dependency on frequency is also explained by Georgiadou and Kleusberg.[10]

Code, Carrier, and SNR Multipath Error Synergy

The code, carrier, and SNR are affected by multipath in different ways. Figure 16 shows the code, carrier, and SNR error patterns in the presence of a multipath signal with a reflection coefficient of 0.7. It can be seen that the code and SNR error patterns are in phase with respect to each other, whereas the carrier-phase error pattern is quadrature phase with respect to the code and SNR errors. The uniform pattern of these errors and their interrelationships is such that if any of these three errors is known, it may be possible to estimate the other two if a suitable relationship can be established among the three.

Figures 17 and 18 show the code, carrier, and SNR multipath errors for satellites 31 and 9, respectively, from the data collected on 20 October 1998. It is clear from Figs. 17 and 18 that the code, carrier, and SNR multipath errors have similar patterns. Generally the code multipath has more prominent oscillations compared to the carrier and SNR errors. This suggests that there is one or more far away reflectors, which play a dominant role in the case of the code. The carrier-phase multipath looks noisier because it was computed by taking double differences between antennas and between satellites, which increases the amount of thermal noise.

The most interesting observation from Figs. 17 and 18 is that the code and SNR multipath errors are of the same phase for both satellites. However, the carrier multipath is phase offset with respect

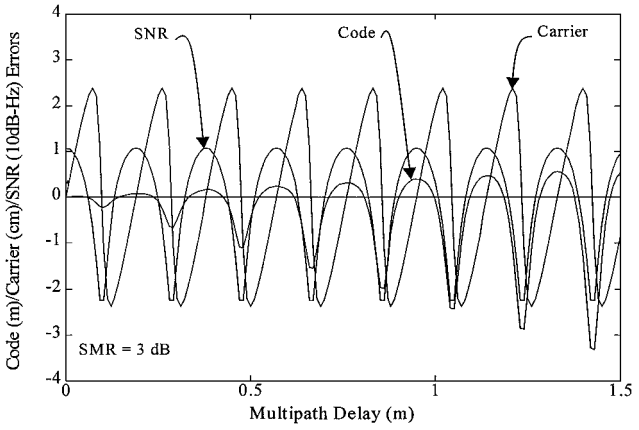

Fig. 16 Code, carrier, and SNR multipath errors due to a reflector with reflection coefficient of 0.7.

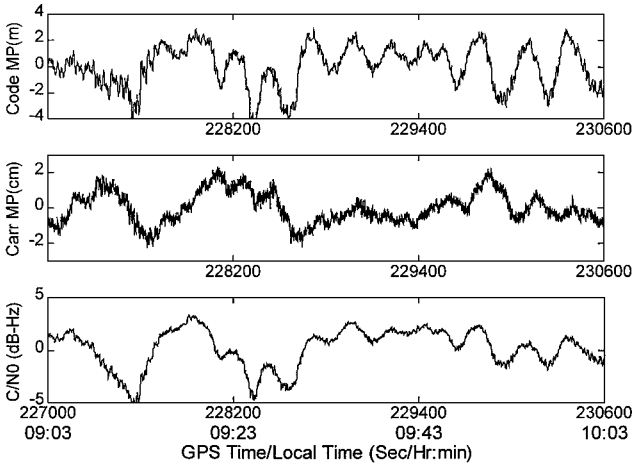

Fig. 17 Code, carrier, and SNR multipath errors for satellite 31 in data collected on 20 Oct. 1998.

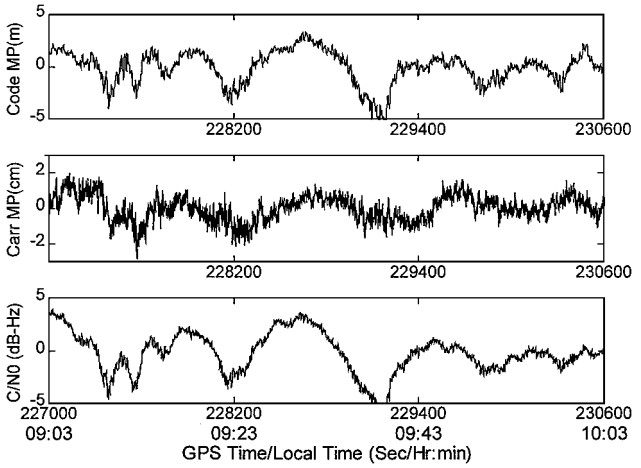

Fig. 18 Code, carrier, and SNR multipath errors for satellite 9 in data collected on 20 Oct. 1998.

to the code and SNR errors. If the carrier multipath is left shifted in time by approximately 2 min, then there is a higher degree of temporal correlation among the code, carrier, and SNR errors. This is in accord with the theoretical and simulated relationships among the code, carrier, and SNR multipath errors.

Conclusions

Multipath is a major source of error for high-accuracy differential code and carrier positioning. Effective multipath mitigation techniques or multipath avoidance requires a sound understanding of its characteristics. In this paper, various code, carrier, and SNR multipath characteristics are analyzed using simulation models and field data.

This paper derives various relationships between multipath parameters such as the multipath amplitude, phase, and frequency with respect to satellite dynamics, antenna–reflector distances, and antenna–reflector geometry. It was found that the presence of multiple reflectors in the environment makes the multipath errors irregular in nature. The location of the reflector plays different roles on code and carrier multipath errors. Distant reflectors play a dominant role for code, whereas close-by reflectors play a dominant role for the carrier. As a result, the multipath error correlation time is different for the code and the carrier. In a complex multipath environment, the correlation time is influenced by the dominant reflector in the environment.

It was also found that the multipath errors in L1 and L2 carriers have similar patterns, but different periods. Further investigations revealed that the code, the carrier, and the SNR multipath errors are phase related. The code and the SNR errors have similar phases, and the carrier multipath is phase offset with respect to the code. This was further confirmed by the field data.

This analysis may be further extended using image theory of electromagnetic signals. The change in signal phase and polarization due to reflection, and its effect on various antennas, requires further research.

Appendix: Computation of Multipath Delay from a Geometrical Perspective

The differential path delay of the multipath signal with respect to the direct signal can be obtained from a geometrical perspective as shown in Fig. A1. Figure A1 is similar to Fig. 2, except that only one antenna and a single reflector case is considered here. This is one of the two scenarios that represent all of the possible scenarios of the antenna–reflector geometry.

In Fig. A1, the direct and reflected signals arrive at the antenna at point O. $P1$ is the point of reflection, and $P11$ is its footprint on the XY plane. The solid lines in Fig. A1 are GPS signals. The dotted lines are on the XY plane and the dashed lines are either slant or vertical. The dotted and dashed lines are drawn for the purpose of analysis only. They are described as follows:

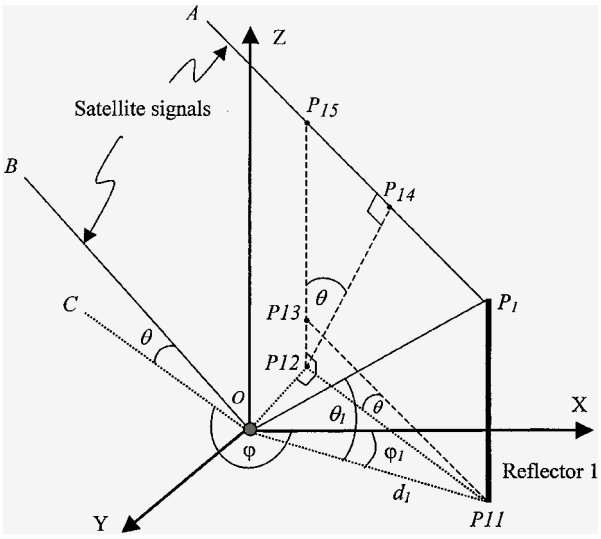

Fig. A1 Direct and reflected signals at an antenna to compute the differential path delay from a geometrical perspective.

1) Draw a dotted line ($OP12$) perpendicular to the projection of the direct signal to the antenna on the XY plane (CO).

2) Draw a dotted line ($P11P12$), which is a projection of the direct signal to the reflector on the XY plane ($AP1$). This intersects the line drawn in step 1 at point $P12$.

3) Draw a dashed line ($P11P13$) from $P11$ with an elevation angle of the direct signal and in the same vertical plane on which the direct signal to the reflector lie.

4) Draw a dashed line ($P12P15$) from point $P12$ and perpendicular to the XY plane. This intersects the line drawn in step 3 at $P13$. This also intersects the direct signal to the reflector at point $P15$. Then $P15P1$ and $P13P11$ are parallel and of equal length.

5) Draw a dashed line ($P12P14$) from point $P12$, which intersects the direct signal to the reflector at point $P14$ orthogonally.

From Fig. A1 it can be observed that the plane containing the points O, $P12$, and $P14$ is a wave front of the direct signal. Therefore, at any point on this plane, the signal will have the same phase. Then the reflected signal relative path delay (or the multipath delay) is equal to $|P14P1 + P1O|$.

Now, from the paralleolgram $P11P13P15P1$,

$$|P15P1| = |P13P11| = |P12P11|/\cos\theta \tag{A1}$$

From the triangle $P11OP12$,

$$\angle OP12P11 = 90 \text{ deg} \tag{A2}$$

$$\angle P11OP12 = \varphi_1 - (\varphi + 90) \tag{A3}$$

$$|OP11| = d_1 \tag{A4}$$

Then,

$$\begin{aligned} |P12P11| &= |OP11| \sin(\angle P11OP12) \\ &= d_1 \sin[\varphi_1 - (\varphi + 90)] \\ &= d_1 \cos(\varphi - \varphi_1) \end{aligned} \tag{A5}$$

Therefore, from Eqs. (1) and (5),

$$|P15P1| = d_1 \cos(\varphi - \varphi_1)/\cos\theta \tag{A6}$$

Now, in the triangle $P12P15P14$

$$\angle P15P14P12 = 90 \text{ deg} \tag{A7}$$

$$\angle P14P12P15 = \theta \tag{A8}$$

$$
\begin{aligned}
|P12P15| &= |P12P13| + |P13P15| \\
&= |P12P13| + |P11P1| \\
&= |P11P12| \tan\theta + d_1 \tan\theta_1 \\
&= d_1 \cos(\varphi - \varphi_1) \tan\theta + d_1 \tan\theta_1 \qquad \text{(A9)}
\end{aligned}
$$

Therefore,

$$
\begin{aligned}
|P15P14| &= |P12P15| \sin\theta \\
&= \{d_1 \cos(\varphi - \varphi_1) \tan\theta + d_1 \tan\theta_1\} \sin\theta \qquad \text{(A10)}
\end{aligned}
$$

Therefore, the differential path delay

$$
\begin{aligned}
|P14P1| + |P1O| &= |P15P1| - |P15P14| + |P1O| \\
&= [d_1 \cos(\varphi - \varphi 1)]/\cos\theta - [d_1 \cos(\varphi - \varphi 1) \tan\theta \\
&+ d_1 \tan\theta_1] \sin\theta + d_1/\cos\theta_1 \\
&= d_1 \cos(\varphi - \varphi 1)/\cos\theta - d_1 \cos(\varphi - \varphi 1) \sin^2\theta/\cos\theta \\
&- d_1 \tan\theta_1 \sin\theta + d_1/\cos\theta_1 \\
&= d_1\{1/\cos\theta_1 - \tan\theta_1 \sin\theta - \cos\theta \cos(\varphi - \varphi_1)\} \qquad \text{(A11)}
\end{aligned}
$$

The same result is obtained for the second reflector shown in Fig. 2.

References

[1]Braasch, M. S., and van Graas, F., "Guidance Accuracy Considerations for Realtime GPS Interferometry," *Proceedings of ION GPS-91*, Inst. of Navigation, Alexandria, VA, 1991, pp. 373–386.

[2]Braasch, M. S., "Multipath Effects," *Global Positioning Systems: Theory and Applications*, edited by B. W. Parkinson and J. J. Spilker, Jr., Vol. 1, AIAA, Reston, VA, 1996, pp. 547–568.

[3]Hagerman, L. L., "Effects of Multipath on Coherent and Non-Coherent PRN Ranging Receiver," Development Planning Div., Aerospace Rept. TOR-0073 (3020-03)-3, The Aerospace Corp., Los Angeles, 1973.

[4]van Nee, R. D. J., *Multipath and Multi-Transmitter Interference in Spread-Spectrum Communication and Navigation Systems*, Delft Univ. Press, Delft, The Netherlands, 1995.

[5]Ray, J. K., and Cannon, M. E., "Characterization of GPS Carrier Phase Multipath," *Proceedings of ION National Technical Meeting*, Inst. of Navigation, Alexandria, VA, 1999, pp. 243–252.

[6]Falkenberg, W., Kielland, P., and Lachapelle, G., "GPS Differential Positioning Technologies for Hydrographic Surveying," *Proceedings of IEEE PLANS*, Inst. of Electrical and Electronics Engineers, New York, 1998, pp. 310–317.

[7]Lachapelle, G., Falkenberg, W., Neufeldt, D., and Keilland, P., "Marine DGPS Using Code and Carrier in Multipath Environment," *Proceedings of ION GPS-89*, Inst. of Navigation, Alexandria, VA, 1989, pp. 343–347.

[8]Cannon, M. E., and Lachapelle, G., "Analysis of a High-Performance C/A-Code GPS Receiver in Kinematic Mode," *Navigation: Journal of The Institute of Navigation*, Vol. 39, No. 3, 1992, pp. 285–300.

[9]Tranquilla, J., and Carr, J., "GPS Multipath Field Observations at Land and Water Sites," *Navigation: Journal of the Institute of Navigation*, Vol. 37, No. 4, 1990, pp. 393–414.

[10]Georgiadou, Y., and Kleusberg, A., "On Carrier Signal Multipath Effects in Relative GPS Positioning," *Manuscripta Geodatica*, Vol. 13, No. 3, 1988, pp. 172–179.

[11]Breeuwer, E., "Modeling and Measuring GPS Multipath Effects," M.Sc. Thesis, Faculty of Electrical Engineering, Delft Univ. of Technology, Delft, The Netherlands, Jan. 1992.

[12]Kee, C., and Parkinson, B. W., "Calibration of Multipath Errors on GPS Pseudorange Measurements," *Proceedings of ION GPS-94*, Inst. of Navigation, Alexandria, VA, 1994, pp. 353–362.

[13]Lachapelle, G., Bruton, A., Henriksen, J., Cannon, M. E., and McMillan, C., "Evaluation of High Performance Multipath Reduction Technologies for Precise DGPS Shipborne Positioning," *The Hydrographic Journal*, Vol. 82, Oct. 1996, pp. 11–17.

[14]Itani, K., Hamada, K., and Hayashi, T., "Development of a Real-Time Multipath Monitor and Experimental Results," *Proceedings of ION GPS-96*, Inst. of Navigation, Alexandria, VA, 1996, pp. 729–733.

[15]Mora-Castro, E. J., "Characterization of the Multipath Effects on the GPS Pseudorange and Carrier Phase Measurements," *Proceedings of ION GPS-98*, Inst. of Navigation, Alexandria, VA, 1998, pp. 1065–1074.

[16]Ward, P., "Satellite Signal Acquisition and Tracking," *Understanding GPS Principles and Applications*, edited by E. D. Kaplan, Artech, Boston, 1996, pp. 119–208.

[17]"GP2021—GPS 12 Channel Correlator with Microprocessor Support Functions," GEC Plessey Semiconductors, U.K., July 1996.

[18]Holmes, J. K., *Coherent Spread Spectrum Systems*, Krieger, Malabar, FL, 1982.

[19]Haykin, S., *An Introduction to Analog and Digital Communication*, Wiley, New York, 1989.

[20]Ford, T., Kunysz, W., Morris, R., Neumann, J., Rooney, J., and Smit, T., "Beeline RT20—A Compact, Medium Precision Positioning System with an Attitude," *Proceedings of ION GPS-97*, Inst. of Navigation, Alexandria, VA, 1997, pp. 687–695.

[21]Ray, J. K., Cannon, M. E., and Fenton, P., "Code Range and Carrier Phase Multipath Mitigation using SNR, Range and Phase Measurements in a Multi-Antenna System," *Proceedings of ION GPS-99*, Inst. of Navigation, Alexandria, VA, 1999, pp. 713–726.

[22]Ray, J. K., "Use of Multiple Antennas to Mitigate Carrier Phase Multipath in Reference Stations," *Proceedings of ION GPS-99*, Inst. of Navigation, Alexandria, VA, 1999, pp. 269–280.

[23]Ray, J. K., Cannon, M. E., and Fenton, P., "Mitigation of Static Carrier Phase Multipath Effects Using Multiple Closely-Spaced Antennas," *Navigation: Journal of The Institute of Navigation*, Vol. 46, No. 3, 1999, pp. 193–202.